IEEE Access
Multidisciplinary ⋮ Rapid Review ⋮ Open Access Journal

Received 15 November 2022, accepted 27 November 2022, date of publication 30 November 2022,
date of current version 5 December 2022.

Digital Object Identifier 10.1109/ACCESS.2022.3225542

RESEARCH ARTICLE

Compact Multilayered Balanced-to-Balanced Dual- and Tri-Band Diplexers Based on Magnetically Coupled Open-Loop Resonators

JOSE L. MEDRÁN DEL RÍO[1], (Graduate Student Member, IEEE), ARMANDO FERNÁNDEZ-PRIETO[1], (Senior Member, IEEE), JESÚS MARTEL[2], (Senior Member, IEEE), RAFAEL R. BOIX[1], (Member, IEEE), AND FRANCISCO MEDINA[1], (Fellow, IEEE)

[1]Departamento de Electrónica y Electromagnetismo, Facultad de Física, Universidad de Sevilla, 41012 Seville, Spain
[2]Departamento de Física Aplicada II, Escuela Técnica Superior de Arquitectura, Universidad de Sevilla, 41012 Seville, Spain

Corresponding author: Armando Fernández-Prieto (armandof@us.es)

This work was supported by MCIN/AEI/10.13039/501100011033 under Grant PID2020-116739GB-I00. The work of Jose L. Medrán del Río was supported in part by MCIN/AEI/10.13039/501100011033 through Research Scholarship under Grant PRE2018-085677, and in part by ESF Investing in Your Future.

ABSTRACT Two new compact balanced-to-balanced diplexers composed of two multiband balanced bandpass filters in a multilayer configuration are proposed in this letter to perform dual- and tri-band responses. The balanced bandpass filters are based on the use of magnetically coupled open-loop resonators. The magnetic coupling results in a strong inherent common-mode rejection, greater than 40 dB within all the dual-band diplexer passbands and greater than 30 dB for the tri-band diplexer passbands. All passbands in both diplexers are close to each other and well separated thanks to the presence of several transmission zeroes between them. Operating frequencies have been selected to be within the L band, used for many applications such as mobile services or satellite navigation. Specifically, the dual-band diplexer passbands are located at 1.08/1.58 GHz and 1.3/1.8 GHz with fractional bandwidths of 7/5.2 % and 7.4/5.5 %, while the tri-band diplexer passbands are located at 1.7/2.2/2.79 GHz and 1.97/2.37/2.95 GHz with fractional bandwidths of 4.1/4.6/3.5 % and 5.6/4.6/3.7 %. Measurements of two different prototypes are provided to validate the obtained simulation results, illustrating in this manner the usefulness of the proposed design methodology.

INDEX TERMS Balanced diplexer, common-mode rejection, dual-band diplexer, L band, microstrip diplexer, multilayer, stripline diplexer, tri-band diplexer.

I. INTRODUCTION

The development in recent years of wireless communications, satellite navigation systems and many other radio communication applications has led to an increase in the demand of multiband devices, such as multiband bandpass filters (BPFs), diplexers, or multiplexers, among many other devices with multiband capabilities. Along with this increase in attention to multiband devices there has also been a growing interest in balanced devices, as they offer well known useful advantages over their single-ended counterparts [1], [2], [3], [4]. These benefits provided by balanced devices lie mainly in their inherent immunity to electromagnetic interference and environmental noise, as well as an improved signal-to-noise ratio which allows for lower voltage operation. The combination of these two features is very interesting from a designer's point of view, as it brings together the advantages of these two highly demanded type of devices. For this reason, multiband differential-mode (DM) devices have attracted a lot of attention in recent years [1], [2], [3], [4], [5], [6], [7], [8], [9], [10], [11], [12], [13], [14], [15], [16]. Diplexers are a type of devices on which researchers have recently focused their attention [17], [18], [19], [20], [21], [22], [23], [24], [25], [26], [27], [28], [29], [30], [31].

The associate editor coordinating the review of this manuscript and approving it for publication was Wenjie Feng.

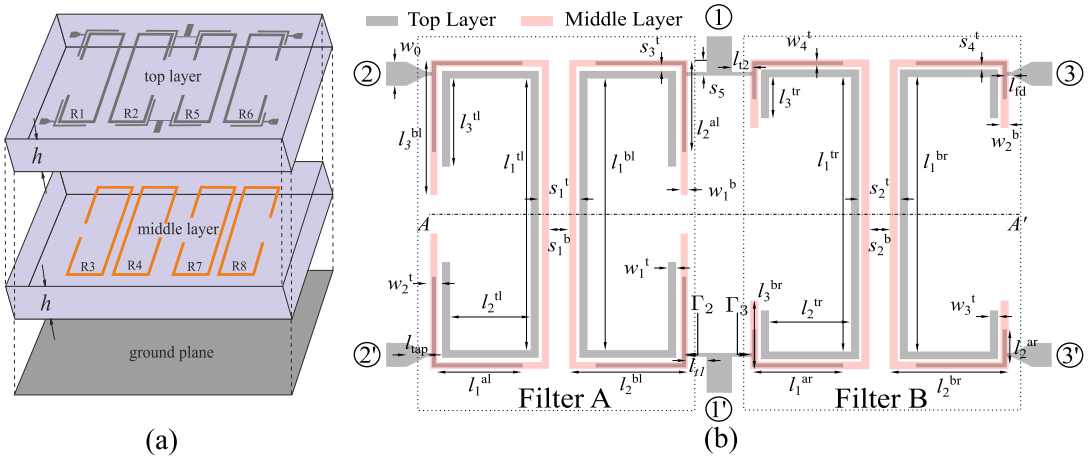

FIGURE 1. (a) 3D-view and (b) top view of the proposed dual-band diplexor. Final dimensions (in mm) are: $w_0 = 2.5$, $w_1^t = 0.8$, $w_2^t = 0.4$, $w_3^t = 0.8$, $w_4^t = 0.4$, $w_1^b = 0.7$, $w_2^b = 0.8$, $l_1^{al} = 8.95$, $l_2^{al} = 9.45$, $l_1^{ar} = 8.95$, $l_2^{ar} = 3.95$, $l_1^{tl} = 28.3$, $l_2^{tl} = 7.9$, $l_3^{tl} = 9.2$, $l_1^{tr} = 28.6$, $l_2^{tr} = 8$, $l_3^{tr} = 4.3$, $l_1^{bl} = 30.8$, $l_2^{bl} = 10.3$, $l_3^{bl} = 13.4$, $l_1^{br} = 30.7$, $l_2^{br} = 10.1$, $l_3^{br} = 6.35$, $l_{tap} = 2$, $l_{fd} = 0.5$, $l_{t1} = 2$, $l_{t2} = 2$, $s_1^t = 4.07$, $s_2^t = 4$, $s_3^t = 0.61$, $s_4^t = 0.45$, $s_1^b = 2.04$, $s_2^b = 2.04$, $s_5 = 1.23$. Substrate parameters: $\varepsilon_r = 3$, $h = 1.016$ mm and $\tan\delta = 0.0013$.

Among them, references [28], [29], [30], and [31] deal with planar dual-band balanced diplexers (DB-BDs). The main features that must be present in a well designed multi-band balanced diplexer are good DM performance, strong common-mode (CM) rejection and high isolation between passbands. Output channels interference must be also low and for this reason high isolation between output ports is also required. The DB-BDs presented in [28], [29], [30], and [31], as the first one proposed in this letter, are designed by combining two individual dual-band bandpass filters (DB-BPFs) to achieve the desired diplexer response. In [28] and [29] the passbands are spaced far apart and the designs do not incorporate transmission zeros (TZs) between the passbands (a very desirable feature for this kind of devices). In [30], the differential passbands are well-defined with high isolation between them but, once again, very spaced apart. On the other hand, common-mode rejection better than 40 dB is provided over a relatively wide bandwidth. In [31], a reflectionless approach is presented where the passbands are very close to each other including TZs between them. However, the common-mode rejection level is limited to 20 dB and the design makes use of resistors to achieve low common-mode in-band input power reflection.

In this paper, two approaches for the design of balanced diplexers (BD) based on simple coupled open-loop resonators are presented. Both structures are based on a multilayer topology composed by two multiband balanced bandpass filters. There are several reasons for choosing to use a multi-layer topology instead of a single-layer approach. Firstly, the use of a multilayer structure allows to achieve a high level of miniaturization, which is a complex task when designing multiplexer. In fact, it is one of the main objectives of this work. Secondly, thanks to the multilayer structure, magnetic coupling between resonators can be used. Indeed, one of the main benefits of the multilayer structure is precisely its flexibility in locating several independent filters with magnetically coupled resonators. This allows for the implementation of filters and diplexers with both multiband operation and inherent common-mode rejection, something that would not be easy for a single layer approach, which would require additional stages to suppress common-mode propagation. The idea of using magnetic coupling to design balanced diplexers was used for the first time in [18] and [20]. However, in [18] and [20] the proposed diplexers were designed to provide one single passband per output. In our paper, we have extended this idea to design diplexers with two and three differential passbands per output channel. For the first approach of this work the dual-band case, the structure features a multilayer microstrip topology with two dual-band balanced bandpass filters (DB-BBPFs) while the tri-band diplexer presents a multilayer stripline topology with two tri-band balanced bandpass filters (TB-BBPFs). The individual filters are based on magnetically coupled resonators, as the one reported in [32]. However, the designs presented in this contribution go beyond the design of two individual balanced dual-band bandpass filters. Here, the T-junction plays a fundamental role since it is optimized to introduce transmission zeros between the passbands in order to improve the selectivity of the devices. Furthermore, thanks to the flexibility in the design of the T-junction, it is possible to extend the idea in [32] to a three layers' structure to design, for the first time to the authors knowledge, a balanced diplexer with three differential passbands per output channel.

In brief, the main features of this design approach are: 1) Compactness, since multilayer approach allows the miniaturization of the device; 2) high selectivity passbands close to each other with TZs between them; 3) strong common-mode suppression over a relatively wide bandwidth; 4) design simplicity, which makes the structure easily adjustable to other frequencies and bandwidths; and 5) scalability, since this structure can be easily modified to accommodate more layers or higher order filters.

II. DUAL-BAND BALANCED DIPLEXER PROTOTYPE

A. GEOMETRIC CONFIGURATION

The proposed structure to implement the DB-BD considered in this contribution is based on a multilayer topology that includes two metalized layers. A 3D-view and a top view of the structure can be seen in Fig. 1. Basically, the DB-BD is composed of two individual 2nd order DB-BBPFs, one constituted by open-loop resonators 1,2,3 and 4 (filter A) and the other by open-loop resonators 5, 6, 7 and 8 (filter B). Feeding structure, which will be described later on, is located on top layer. The coupling scheme of each DB-BBPFs is represented in Figs.2 (a) and (c) in which we can observe the direct coupling paths (solid lines) and the cross-coupling paths (dashed lines). However, for simplicity, in the design of the DB-BBPFs we have neglected the coupling between the resonators of different layers. This approximation is reasonable because the resonance frequency is different for the resonators of the top layer and the resonators of the middle layer. Therefore, as a first approximation, each passband of filters A or B is mainly controlled by the pair of resonators located on the same layer of the structure (the center frequency depends on the resonator size, the fractional bandwidth, Δ, depends on the coupling coefficients M_{ij} and the specific matching level at the input and output ports can be achieved by the external quality factors $Q^{i}_{\mathrm{EI(EO)}}$ -see Fig. 2-). In other words, each DB-BBPF is composed of two single-band balanced bandpass filters (SB-BBPF) that can be considered almost completely independent and, therefore, be designed following the well-known procedure explained in [33] for single-band bandpass filters whose corresponding coupling scheme is the one in Fig. 2 (b) and (d). Nevertheless, please note that each pair of SB-BBPFs are connected to a common source and load (see Fig. 2) so the key point in the design is to achieve the required external quality factors for the two SB-BBPFs in an independent way. With that purpose in mind, the inductive feeding structure used in [32] has been modified to a capacitive one to better adjust the excitation of resonators on different layers. Top layer resonators are excited by means of the edge-gap capacitances controlled by geometrical parameters (referring to Fig. 1) s^{t}_{3} and s^{t}_{4} for $22'$ and $33'$ output channels, respectively, while middle layer resonators are excited by means of broadside capacitances whose values are controlled by the length and width of the feeding arms; w^{t}_{2} and l^{al}_{2} for 22' output channel and w^{t}_{4} and l^{ar}_{2} for 33' output channel, respectively. Thanks to the versatility of this structure provided by the feeding scheme (edge-gap capacitance for resonators on top layer and broadside capacitance for resonators on middle layer), modifications may be included to increase the order of the filters, the number of layers or the number os passbands. This will be demonstrated in section III.

Since the resonators used to create the passbands are coupled across the straight sections carrying a high electrical current, DM coupling is mainly magnetic as discussed in [34]. For DM, the symmetry plane AA' (see Fig. 1 (b)) behaves as an electric wall (virtual short-circuit). This leads to a high current distribution at the resonance frequency. High current

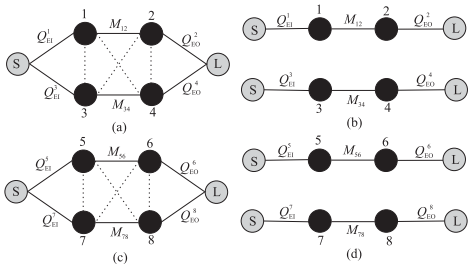

FIGURE 2. Coupling scheme for the design of each individual DB-BBPFs of the proposed diplexer (a) Filter A; (b) the two SB-BBPFs used to design filter A as first approximation; (c) filter B; (d) the two SB-BBPFs used to design filter B as first approximation.

means strong magnetic field which is the bridge that transmits DM between resonators. On the contrary, for CM the symmetry plane AA' is a magnetic wall (virtual open-circuit). In this case, electrical current level is low which means that open-loop resonators are weekly excited. This results in a poor CM transmission. This description is just qualitative and we refer the interested reader to [34] for a deeper discussion on DM and CM coupling schemes.

Returning to the structure under study, a T-junction has been implemented on the top layer (input channel $11'$) with the purpose of enforcing the diplexing response. In the design of this T-junction two DM targets have been prioritized: First one is to preserve the external quality factors obtained for the individual DB-BBPFs which ensures no degradation of DM performance; second one is the introduction of several transmission zeros (TZs) between the differential passbands of both output channels. In Fig. 1 (b) we have shown the reflection coefficients Γ_2 and Γ_3 seen from the feeding points of filter A (channel $22'$) and filter B (channel $33'$), respectively. The T-junction is also designed in such a way that at the center frequencies of the DM passbands of filter A ($f^{\mathrm{c}}_{\mathrm{A1}}$ and $f^{\mathrm{c}}_{\mathrm{A2}}$), the amplitude of the input reflection coefficient $|\Gamma_2|$ is approximately 0 while $|\Gamma_3|$ is close to 1, leading to the appearance of TZs in the output channel $33'$ at those frequencies. Likewise, TZs in channel $22'$ are obtained at the center frequencies of the passbands of filter B ($f^{\mathrm{c}}_{\mathrm{B1}}$ and $f^{\mathrm{c}}_{\mathrm{B2}}$) for which $|\Gamma_2| \approx 1$ and $|\Gamma_3| \approx 0$ [18], [20].

B. DESIGN PROCEDURE

As previously mentioned, each channel DB-BBPF will be treated as the combination of two SB-BBPF based on two magnetically coupled open-loop resonators excited with the same input structure (see Fig. 2). In this work, each SB-BBPF will be designed with an order $n = 2$ maximally flat response. For this transfer function, the values of the corresponding low-pass prototype elements are $g_0 = g_3 = 1$ and $g_1 = g_2 = 1.4142$. Filters specifications (center frequencies of the passbands and fractional bandwidths), required coupling coefficients and external quality factors can be found in Table 1. The coupling coefficients and external quality factors have been extracted from the well-known equations for the coupling coefficients M_{ij}, the input (Q_{EI}) and the output (Q_{EO}) external quality factors of a filter of order n and frac-

TABLE 1. SB-BBPFs specifications, required coupling coefficients and external quality factors for the DB-BD.

	Filter A (Channel 22')	Filter B (Channel 33')
Top layer	$f_{A1}^{c} = 1.54\,\text{GHz}$ $\Delta_{A1} = 5\%$ $Q_{EI}^{1} = Q_{EO}^{2} = 28.28$ $M_{12} = 0.042$	$f_{B1}^{c} = 1.75\,\text{GHz}$ $\Delta_{B1} = 5\%$ $Q_{EI}^{5} = Q_{EO}^{6} = 28.28$ $M_{56} = 0.042$
Middle layer	$f_{A2}^{c} = 1.06\,\text{GHz}$ $\Delta_{A2} = 7\%$ $Q_{EI}^{3} = Q_{EO}^{4} = 20.2$ $M_{34} = 0.059$	$f_{B2}^{c} = 1.28\,\text{GHz}$ $\Delta_{B2} = 7\%$ $Q_{EI}^{7} = Q_{EO}^{8} = 20.2$ $M_{78} = 0.059$

tional bandwidth Δ [33]:

$$M_{i,i+1} = \frac{\Delta}{\sqrt{g_i g_{i+1}}}, \quad \text{for } i = 1, \ldots, n-1 \tag{1}$$

$$Q_{EI} = \frac{g_0 g_1}{\Delta} \tag{2}$$

$$Q_{EO} = \frac{g_n g_{n+1}}{\Delta} \tag{3}$$

The substrate chosen to implement the structure under study is the same for both layers, namely *Rogers CLTE-AT* whose characteristics are: $\varepsilon_r = 3$, thickness $h = 1.016$ mm and $\tan\delta = 0.0013$ (see Fig. 1).

Although the topology of the DB-BBPFs was first proposed in [32], no theoretical framework was given. In this paper we provide an step-by-step design procedure for the DB-BBPF composing each diplexer output channel and for the final DB-BD, which can be extended for more complex structures including more layers and thus more differential passbands (see section III). The design process followed to implement the final structure consists of the following steps:

1) Finding the dimensions of the individual resonators:
The operation frequency of the filter is mainly controlled by the physical length of the resonators. Since the resonators chosen are simple open-loop resonators, their length is approximately half of the guided wavelength at their respective resonant frequencies (f_{A1}^{c} for resonators #1 and #2, f_{A2}^{c} for resonators #3 and #4, f_{B1}^{c} for resonators #5 and #6 and f_{B2}^{c} for resonators #7 and #8). To find the resonator dimensions, classical transmission lines calculators can be employed. In our case, the package *Linecalc* incorporated in ADS Keysight *Momentum* is used [35].
2) Imposing the required coupling coefficients and the external quality factors for the SB-BBPFs involved:
Once the physical dimensions of the resonators have been found, the next step consists of imposing the required coupling coefficients between the coupled resonators extracted from the specific fractional bandwidths. The coupling level between resonators is mainly controlled by the gap distance between the resonators (s_1^t and s_1^b for filter A), in such a way that smaller gap distances lead to greater coupling levels (and larger fractional bandwidths). For each DB-BBPF the extraction of the coupling coefficient M_{ij} is carried out separately for its two individual SB-BBPFs following the standard procedure in [33]. On the other hand, the matching level is related to the external quality factor which is controlled by the filters feeding schemes. In our case, all feeding schemes are capacitive. Specifically, excitation capacitances are edge-gap type for the top layer resonators and broadside type for the resonators in the middle layer. The physical parameters governing these capacitances for filter A (see Fig. 1) are the length of the feeding arms, l_1^{al}, l_2^{al} and s_3^t. Specifically, l_1^{al} and l_2^{al} have influence on $Q_{EI(EO)}^{i}$ of both layers while s_3^t mainly affects to the values of $Q_{EI(EO)}^{i}$ on top layer resonators. Contrary to the case of coupling coefficients, since the same feeding structure is used to excite both the SB-BBPFs of different layers, to extract the external quality factors $Q_{EI(EO)}^{i}$ we have considered the whole structure itself, i.e., with both input resonators of each layer filter present at the same time. Design curves for the design of filter A are depicted in Fig. 3 (for coupling coefficients M_{12} and M_{34}) and in Fig. 4 (for the external quality factors $Q_{EI}^{1} = Q_{EO}^{2}$ and $Q_{EI}^{3} = Q_{EO}^{4}$). Similar procedure has been followed for the case of filter B.

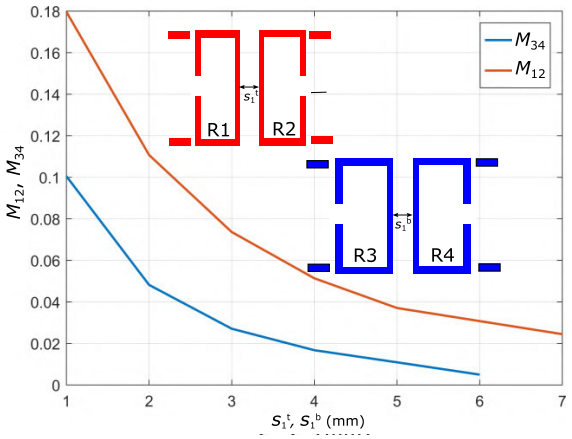

FIGURE 3. Coupling coefficients design curves for the channel 22' (filter A) in Fig. 1 (b) with respect to resonators' separation gap. M_{12} is representing versus s_1^t and M_{34} is representing versus s_1^b.

The initial values for the physical dimensions that allow implementing the theoretical coupling coefficients and external quality factors corresponding to filter A (see Table 1) extracted by using Fig. 3 and Fig. 4 are shown in Table 2. These values have been used as seeds in an optimization tuning process that has been carried out to more accurately obtain both the fractional bandwidths and the matching level set by the SB-BBPFs specifications. The final dimensions of the optimization process are also included in Table 2, where we observe a very good agreement between the initial and final values. This confirms that our approximation of neglecting the coupling between the resonators in different layers works reasonably well. It is worth noting that the dimensions of the resonators do not require adjustment

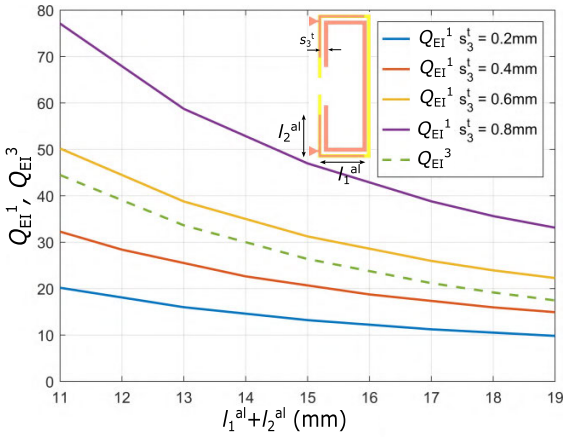

FIGURE 4. External quality factors ($Q_{EI}^1 = Q_{EO}^2$ and $Q_{EI}^3 = Q_{EO}^4$) design curves for channel 22′ (Filter A) in Fig. 1 versus the whole length of the top feeding arms ($l_1^{al} + l_2^{al}$). In the case of Q_{EI}^1 we have considered also its dependence on the gap distance s_3^t.

TABLE 2. Theoretical and optimized values for DB-BPF on channel 22′ (Filter A).

	Initial Values (mm)	Optimized Values (mm)
$l_1^{al} + l_2^{al}$	17.49	17.98
s_3^t	0.65	0.61
s_1^t	5.01	4.07
s_1^b	1.98	2.04

and the only optimized parameters are those shown in Table 2.

3) Join both bandpass filters by means of a suitable T-junction:
Once the two DB-BBPF composing each output channel of the balanced diplexer has been completely designed, the last step in the design process is to connect them using a T-junction. The branch lengths of this T-junction, l_{t1} and l_{t2}, have been used to adjust the the matching levels of the diplexer passbands as explained in [20], since after joining both DB-BPFs there will be a minor disturbance in the matching levels that needs to be corrected. These effects are shown in Fig. 5, where the simulated return loss has been plotted for several values of l_{t1} and l_{t2}.
Additionally, as mentioned before, the connection between the T-junction and the filters feeding lines (which is controlled by distance s_5) has been selected so that TZs are introduced in each output channel at the passband center frequencies of the other output channel.

Following this process, final dimensions can be set (see caption in Fig. 1). The simulated electromagnetic response of the DB-BD has been obtained using ADS Momentum from Keysight [35]. Results are displayed in Fig. 6. DM shows four well-defined passbands. As expected, due to the T-junction design, the differential passbands are separated by TZs in both output channels. To better illustrate this phenomenon, in Fig. 7 we depict the electric current distribution at two different frequencies corresponding to two different channel

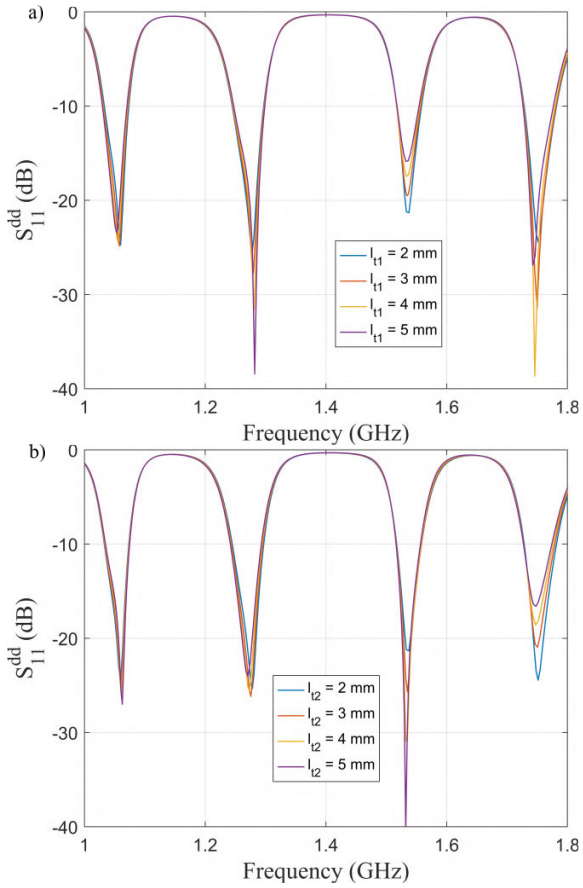

FIGURE 5. Matching level of the differential passbands when adjusting the length of the branch of the T-junction. a) l_{t2} is fixed at 2 mm and b) l_{t1} is fixed at 2 mm.

TZs. Notice that in Fig. 7 the TZ frequency in channel 22′ corresponds with the center frequency of channel 33′ and viceversa. This fact demonstrates that currents only flow through the branch of the diplexer that is excited at that given frequency without interfering with the other branch. For CM, a suppression level better than 40 dB in all DM passbands is observed. This response will be tested later in the next section with a prototype that has been manufactured to corroborate these results.

C. EXPERIMENTAL RESULTS AND DISCUSSION

Following the aforementioned steps, a DB-BD prototype has been manufactured to verify the results obtained in Fig. 6. Measurements are depicted in Fig. 8 where four DM passbands are present with the following characteristics: for channel 22′, passbands are centered at 1.08 GHz and 1.58 GHz with $\Delta's$ of 7 % and 5.2 % and insertion loss (IL) of 1.91 dB and 1.35 dB, respectively. In the case of channel 33′, passbands are centered at 1.3 GHz and 1.8 GHz with $\Delta's$ of 7.4 % and 5.5 % and IL of 1.2 dB and 1.16 dB, respectively. Good agreement between simulations and experiments is demonstrated. There is a slight shift in the measured frequency response that is caused by two reasons: First, the value of the dielectric constant of the substrate used is not exactly the same as $\varepsilon_r = 3$. Second, the presence of small

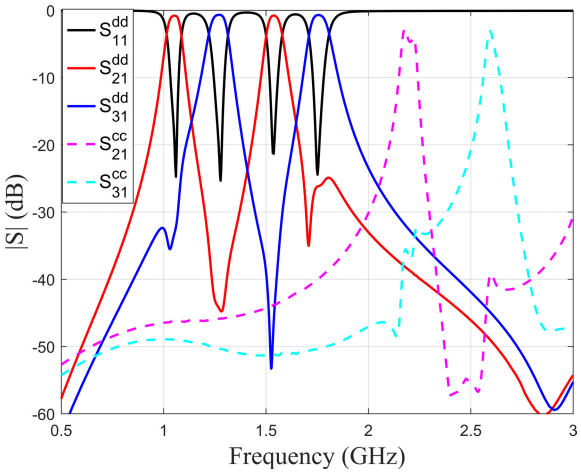

FIGURE 6. Simulated response of the diplexer presented in Fig. 1.

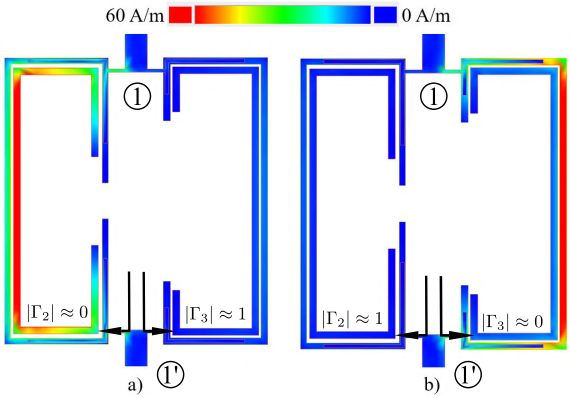

FIGURE 7. DM electric currents distribution at a) f^c_{A1}=1.54 GHz (TZ on channel 33′) and b) f^c_{B2}=1.28 GHz (TZ on channel 22′).

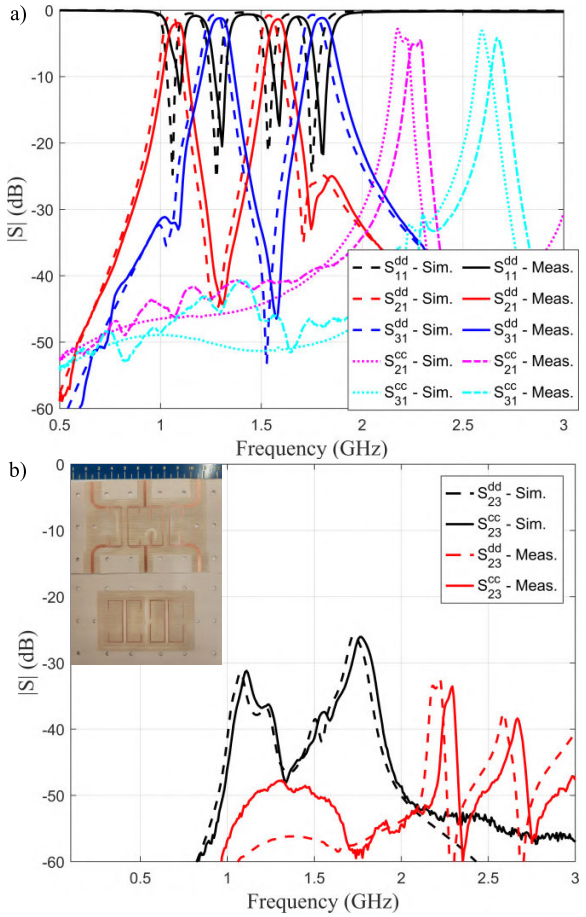

FIGURE 8. Measured and simulated response of the proposed dual-band diplexer. a) CM and DM S_{11}, S_{21} and S_{31} S-parameters and b) CM and DM S_{23} parameter.

air gaps that may appear between the two layers during the manufacturing process, which modify the effective relative permittivity. A comparison with other DB-BD reported in the literature is presented in Table 3, the table is composed by DB-BD designed in microstrip technology except [24], which is designed as a dielectric resonator. From the table it can be inferred that the proposed design has competitive features when compared to other diplexers, standing out the small size of our structure.

III. TRIBAND DIPLEXER PROTOTYPE

A. GEOMETRIC PARAMETERS AND DESIGN

In this section, the idea proposed above will be extended to implement a multilayer tri-band balanced diplexer (TB-BD) with good DM performance and strong CM rejection. To the authors' knowledge, no differential diplexer with six differential passbands (three per output channel) has been reported before. The structure proposed to implement the TB-BD considered in this paper is based on a multilayer topology consisting of four metalized layers stacked to build up a stripline circuit. A 3D and a top view of the structure layout can be seen in Fig. 9. In this case, the TB-BD is composed by two tri-band balanced bandpass filters (TB-BBPF); filter A (corresponding to the channel 22′) and filter B (corresponding to the channel 33′) that are connected by a T-junction. These two TB-BBPFs are in turn made up of three SB-BBPF composed of two coupled open-loop resonators stacked in different layers sharing the same feeding through the input port 11′ (see coupling scheme represented in Fig. 10). With this prototype we demonstrate the scalability of the original design of the DB-BD adding a new layer to achieve an extra passband per branch of the diplexer. To ensure good coupling between the resonators on the same layer of the structure, a stripline configuration is chosen. This reduces radiation losses and provides low level of electromagnetic coupling between resonators located on different layers. Recall that in our design methodoloy cross-couplings are supposed to be negligible.

The design process is identical to that of the DB-BD, with the difference that the feeding is now located in the middle layer of the structure. In this regard, SB-BBPFs in the middle layer are excited by edge-gap capacitances, while SB-BBPFs in the top and bottom layers are excited by broadside capacitances. The individual SB-BBPFs that make up the structure are still 2^{nd} order filters based on magnetically coupled open-loop resonators and the explanation regarding the reduction of CM transmission is still valid for this configuration.Design specifications are provided in

TABLE 3. Comparison with previously reported balanced dual-band diplexers.

Ref.	Size ($\lambda_g^x \times \lambda_g^y \times \lambda_g^z$)∗	Tech.	Filter order	Differential-Mode				Common-Mode		
				f_0^d (GHz)	3-dB FBW (%)	IL @f_0^d (dB)	B-to-B TZ	CMRR @f_0^d (dB)	$\lvert S_{21}^{cc}\rvert > 40$ dB (GHz)	$\lvert S_{31}^{cc}\rvert > 40$ dB (GHz)
[24]	0.58 x 0.23 x 0.32	D.R ⊙	2	3.51/3.71 - 3.65/3.84	0.9/0.4 - 0.6/0.7	0.39/0.75 - 0.61/0.48	2 PC†	50/50 - 50/50	3.3-4.1	3.3-4.1
[28]	N/A ‡	MS1L ⊘	3	1.91/2.46 - 5.29/5.88	9.4/8.9 - 11.2/10.4	1.7/1.59 - 1.67/1.54	No	38/26 - 39/40	1-2.2 / 5.4-8	1-2.9 / 5.8-8
[29]	1.03 x 0.81 x 0.011	MS1L	2	2.41/5.28 - 3.25/4.84	2.5/1.9 - 1.9/1.6	2.62/2.7 - 2.9/2.6	No	47.5/27.5 - 44/45	1.75-3.2 / 3.4-3.8	1.75-4.4 / 4.75-6
[30]	1.41 x 0.68 x 0.011	MS1L	3	1.92/5.25 - 2.45/5.81	7.9/4 - 6.5/3.4	1.38/1.52 - 1.6/1.8	4 PC	77/50.5 - 60.6/46	1-5.7	1-7
[31]	2.8 x 0.93 x 0.012	MS1L	3	1.51/2.41 - 1.92/2.85	27.4/14.2 - 20.1/11.7	0.55/1.09 - 0.86/1.36	3 PC	19.5/32 - 27.5/28	1.84-2.16	2.22-3.48
This	0.32 x 0.18 x 0.013	MS2L •	2	1.08/1.58 - 1.3/1.8	7/5.2 - 7.4/5.5	1.91/1.35 - 1.2/1.16	3 PC	43.1/39.7 - 44.4/46.4	0.1-1.71	0.1-2.22

∗ Guided wavelength (λ_g) at lowest operation frequency (f_0^d) // † Per channel // ‡ Not available // ⊙ Dielectric Resonator // ⊘ Microstrip 1 Layer // • Microstrip 2 Layers

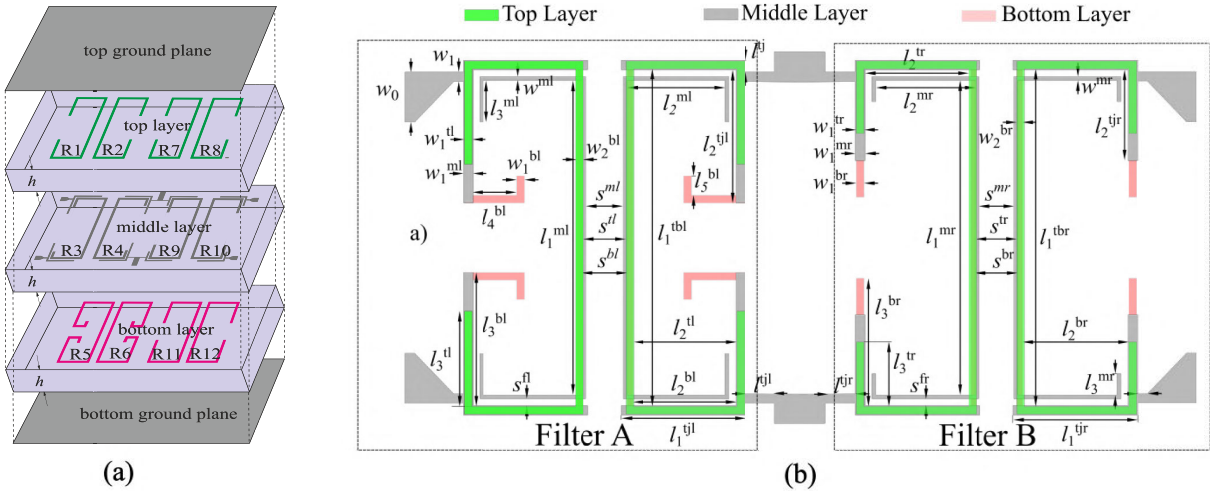

FIGURE 9. a) Layout of the multilayer structure, accompanied by b) the cross-sectional view of the structure and c) the coupling scheme between resonators. Dimensions (in mm) are: $w_0 = 2.6$, $w_1 = 0.5$, $w^{ml} = 0.5$, $w^{mr} = 0.5$, $w_1^{ml} = 0.2$, $w_1^{mr} = 0.2$, $w_1^{tl} = 0.4$, $w_1^{tr} = 0.4$, $w_1^{bl} = 0.4$, $w_2^{bl} = 0.3$, $w_1^{br} = 0.4$, $w_2^{br} = 0.3$, $l_1^{ml} = 16.3$, $l_2^{ml} = 5.05$, $l_3^{ml} = 2.15$, $l_1^{mr} = 16.3$, $l_2^{mr} = 5.1$, $l_3^{mr} = 1.1$, $l_1^{tbl} = 17.5$, $l_2^{tl} = 5.3$, $l_3^{tl} = 4.95$, $l_1^{tbr} = 17.5$, $l_2^{tr} = 5.35$, $l_3^{tr} = 3.35$, $l_2^{bl} = 5.35$, $l_3^{bl} = 6.55$, $l_4^{bl} = 2.3$, $l_5^{bl} = 1$, $l_2^{br} = 5.45$, $l_3^{br} = 6.65$, $l^{tj} = 0.61$, $l^{tjl} = 0.5$, $l^{tjr} = 0.5$, $l_1^{tjl} = 6.4$, $l_2^{tjl} = 6.9$, $l_1^{tjl} = 6.4$, $l_2^{tjl} = 4.71$, $s^{fl} = 0.35$, $s^{fr} = 0.35$, $s_1^{ml} = 1.9$, $s_1^{tl} = 2.2$, $s_1^{bl} = 2.3$, $s_1^{mr} = 1.8$, $s_1^{tr} = 2.1$, $s_1^{br} = 2.1$. Substrate parameters: $\varepsilon_r = 3$, $h = 1.016$ mm and $\tan\delta = 0.0013$.

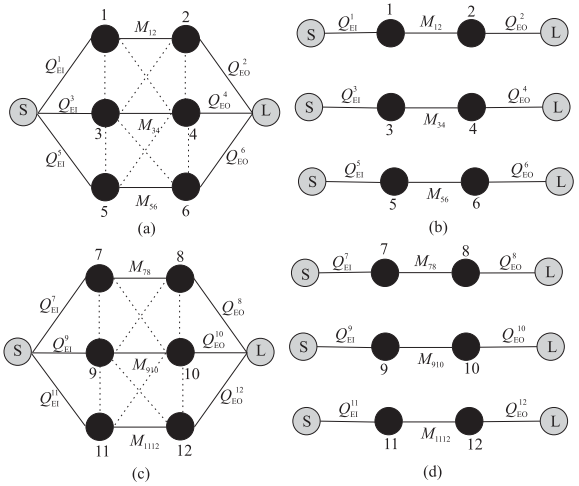

FIGURE 10. Coupling scheme for the design of each individual TB-BBPFs of the proposed TB-BD (a) Filter A; (b) the three SB-BBPFs used to design filter A as first approximation; (c) filter B; (d) the three SB-BBPFs used to design filter B as first approximation.

Table 4. Following a design process very similar to the one described for DB-BD, we have calculated the final dimensions that are shown in the caption of Fig. 9. As an example to show the versatility of the design we provide two different figures that reveal the independence between passbands and the designer's leeway to adjust the device to different specifications. In Fig. 11 the length of the resonators 11-12 is modified while keeping the rest of the parameters unchanged. This allows to display the evolution of the resonance frequency of the specified passband, which, as mentioned above, follows the half-wavelength rule for open-loop resonators. Fig. 12 demonstrates the physical application of the coupling factor variation discussed for the dual-band approach, linking this value to a physical parameter. In this case, such parameter is the gap between resonators 11-12, denoted as s^{br}. No other parameter has been modifided. As shown in the examples, both the frequency and Δ of the diplexer passbands can be changed within a limited range, without interfering with the other passbands of the device. This analysis can be extended to the previous dual-band case. Again, the substrate chosen to implement the proposed TB-BD in this paper is the *Rogers CLTE-AT* for all layers, with dielectric constant $\varepsilon_r = 3$, thickness $h = 1.016$ mm and $\tan\delta = 0.0013$.

B. SIMULATED AND EXPERIMENTAL RESULTS

Simulated results for this balanced multi-band diplexer, depicted in Fig. 13, show six well-defined DM passbands, three per branch of the diplexer, very close to each other and with TZs between them. It is important to note that the proposed diplexer is able to allocate six differential passbands with good band-to-band isolation within a frequency range

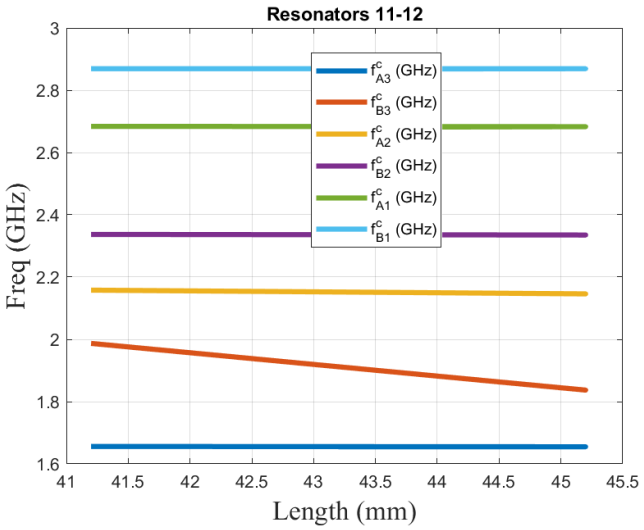

FIGURE 11. Frequency tuning for the passband controlled by the length of the resonators 11-12.

TABLE 4. SB-BBPFs specifications, required coupling coefficients and external quality factors for the TB-BD.

	Filter A (Channel 22')	Filter B (Channel 33')
Middle Layer	$f^c_{A1} = 2.66$ GHz $\Delta_{A1} = 3.5\%$ $Q^1_{EI} = Q^2_{EO} = 40.4$ $M_{12} = 0.029$	$f^c_{B1} = 2.85$ GHz $\Delta_{B1} = 3.5\%$ $Q^7_{EI} = Q^8_{EO} = 40.4$ $M_{78} = 0.029$
Top Layer	$f^c_{A2} = 2.14$ GHz $\Delta_{A2} = 4\%$ $Q^3_{EI} = Q^4_{EO} = 35.35$ $M_{34} = 0.034$	$f_{B2} = 2.32$ GHz $\Delta_{B2} = 4\%$ $Q^9_{EI} = Q^{10}_{EO} = 35.35$ $M_{910} = 0.034$
Bottom Layer	$f^c_{A3} = 1.65$ GHz $\Delta_{A3} = 4\%$ $Q^5_{EI} = Q^6_{EO} = 35.35$ $M_{56} = 0.034$	$f^c_{B3} = 1.9$ GHz $\Delta_{B3} = 5\%$ $Q^{11}_{EI} = Q^{12}_{EO} = 28.28$ $M_{1112} = 0.042$

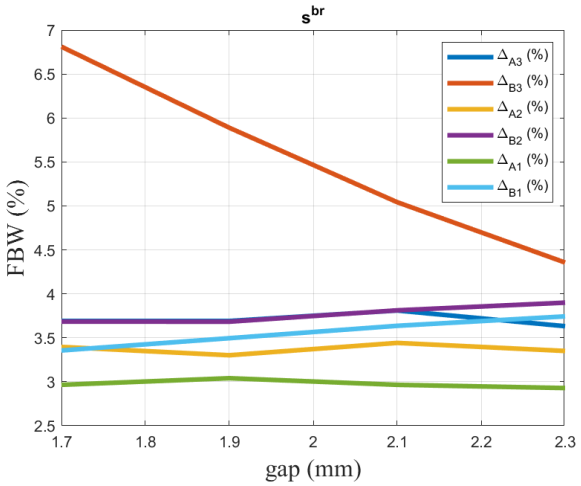

FIGURE 12. FBW tuning for the passband controlled by the physical parameter s^{br}.

of just 1.2 GHz bandwidth. Furthermore, good CM rejection (greater than 30 dB) is observed in all passbands. In order to verify that simulated results are correct, a prototype of the structure in Fig. 9 has been fabricated and measured.

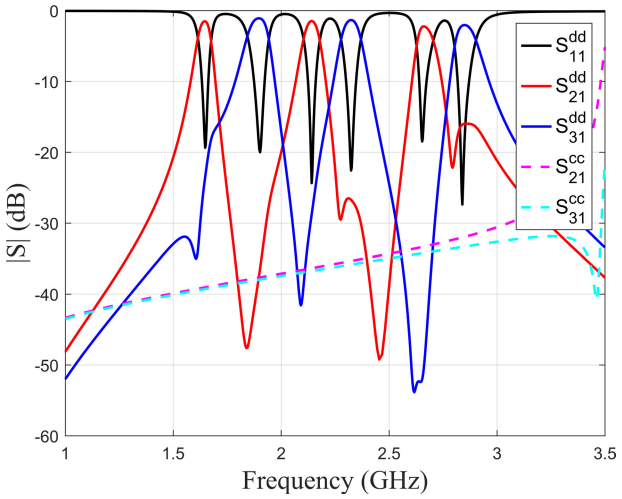

FIGURE 13. Simulated response of the diplexer presented in Fig. 9.

Measured results of the TB-BD designed above are shown in Fig. 14. According to this figure, the proposed design provides six differential passbands with following characteristics: for channel 22′ passbands are centered at 1.7 GHz, 2.2 GHz and 2.79 GHz, with $\Delta's$ of 4.1 %, 4.6 % and 3.5 % and IL of 2.3 dB, 2.3 dB, and 3.1 dB, respectively. For channel 33′, passbands are centered at 1.97 GHz, 2.37 GHz and 2.95 GHz with $\Delta's$ of 5.6 %, 4.6 % and 3.7 % and IL of 1.8 dB, 2.1 dB and 2.9 dB, respectively. The total area occupied by the TB-BD, in terms of the guided wavelength λ_g at the lowest operation frequency, is $0.25\lambda^x_g \times 0.13\lambda^y_g$. Regarding CM, it is observed a rejection level greater than 40 dB between 1 GHz and 2.25 GHz, and greater than 30 dB between 2.25 GHz and 3.25 GHz. Channel-to-channel isolation measurements also provided good results, demonstrating more than -40 dB for CM and -20 dB or more for DM in the whole frequency range.

It is important to note that since the manufacturing process followed to implement this prototype is the same as the one used for the DB-BD case (i.e., multilayer lamination has been performed by using plastic screews), slight frequency shifts are inevitable for the measured center frequencies due to the presence of small air-gaps. Furthermore, for this multilayer structure, discrepancies between simulations and measurements can also be explained in terms of the chosen measurement set-up. As explained above and as can be observed in the prototype pictures presented in the inset of Fig. 14, the TB-BD can be considered a stripline structure, since all resonators are sandwiched between a top and a bottom ground plane. Nevertheless, to measure the response of the prototype it is necessary to include a transition between stripline and microstrip in order to allow the measurement process (see Fig. 14 b) inset). This transition between stripline-to-microstrip technology is not included in the simulated results and may introduce losses and missmatching in the original design. However, taking into account the complexity of the structure and the *homemade lamination* process, measured results show a very good agreement with simulated ones. To the authors' knowledge, this is the first TB-BD presented

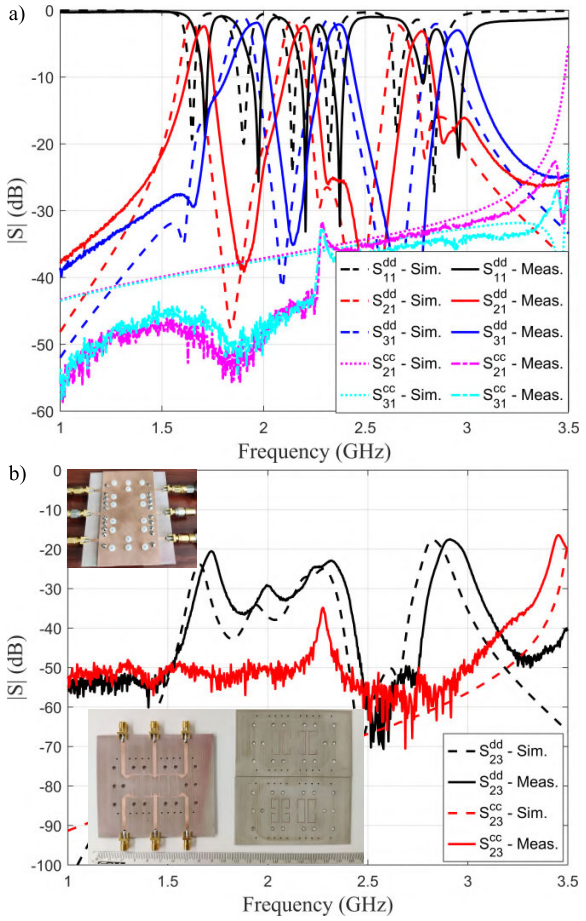

FIGURE 14. Measured and simulated response of the proposed tri-band diplexer. a) CM and DM S_{11}, S_{21} and S_{31} parameters and b) CM and DM S_{23} parameter.

in planar technology, therefore, there are no other designs to compare the performance of our structure.

IV. CONCLUSION

In this paper, a new approach to design balanced-to-balanced diplexers with intrinsic common-mode suppression has been introduced. Two new designs have been proposed, a dual-band and a tri-band balanced diplexers. Both of them are based on multilayer topology, allowing for minituarization and magnetic coupling between resonators providing inherent common-mode rejection. Microstrip technology has been used for the dual-band case and stripline technology was chosen for the tri-band diplexer. Each metalized layer is composed of two pairs of magnetically coupled open-loop resonators that confer a high common-mode rejection without needing to add external elements to the original design. The main features displayed are: 1) very compact size compared to other designs reported in the literature; 2) possibility of closely spaced differential-passbands isolated by transmission zeros on each channel; 3) very low common-mode transmission in the bandwidth of interest and 4) versatility, the design is easily adjusted to host more layers to accommodate more passbands and it is also possible to employ higher order filters.

REFERENCES

[1] F. Martin, L. Zhu, J. Hong, and F. Medina, *Balanced Microwave Filters*. New York, NY, USA: Wiley, 2018.

[2] F. Martin, J. Naqui, A. Fernandez-Prieto, P. Velez, J. Bonache, J. Martel, and F. Medina, "The beauty of symmetry: Common-mode rejection filters for high-speed interconnects and band microwave circuits," *IEEE Microw. Mag.*, vol. 18, no. 1, pp. 42–55, Jan. 2017.

[3] A. Arbelaez-Nieto, E. Cruz-Perez, J.-L. Olvera-Cervantes, A. Corona-Chavez, and H. Lobato-Morales, "The perfect balance—A design procedure for balanced bandpass filters," *IEEE Microw. Mag.*, vol. 16, no. 10, pp. 54–65, Nov. 2015.

[4] W. Feng, W. Che, and Q. Xue, "The proper balance: Overview of microstrip wideband balance circuits with wideband common mode suppression," *IEEE Microw. Mag.*, vol. 16, no. 5, pp. 55–68, Jun. 2015.

[5] Z. Li, F. Wei, B. Liu, and X. W. Shi, "Design of balanced wideband BPF based on tri-mode slotline resonators," *IEEE Trans. Circuits Syst. II, Exp. Briefs*, vol. 69, no. 6, pp. 2767–2771, Jun. 2022.

[6] Z.-A. Ouyang, L. Zhu, and L.-L. Qiu, "Wideband balanced filters with intrinsic common-mode suppression on coplanar stripline-based multi-mode resonators," *IEEE Trans. Circuits Syst. I, Reg. Papers*, vol. 69, no. 6, pp. 2263–2275, Jun. 2022.

[7] Y. Zhang, Y. Wu, W. Wang, and J. Yan, "High-performance common- and differential-mode reflectionless balanced band-pass filter using coupled ring resonator," *IEEE Trans. Circuits Syst. II, Exp. Briefs*, vol. 69, no. 3, pp. 974–978, Mar. 2022.

[8] Z. Zhang, G. Zhang, Z. Liu, W. Tang, and J. Yang, "Compact balanced bandpass filter based on equilateral triangular patch resonator," *IEEE Trans. Circuits Syst. II, Exp. Briefs*, vol. 69, no. 1, pp. 90–93, Jan. 2022.

[9] F. Wei, C. Y. Zhang, C. Zeng, and X. W. Shi, "A reconfigurable balanced dual-band bandpass filter with constant absolute bandwidth and high selectivity," *IEEE Trans. Microw. Theory Techn.*, vol. 69, no. 9, pp. 4029–4040, Sep. 2021.

[10] Z.-A. Ouyang, L. Zhu, and L.-L. Qiu, "Wideband balanced filters with intrinsic common-mode suppression using coplanar strip double-sided shunt-stub structures," *IEEE Trans. Microw. Theory Techn.*, vol. 69, no. 8, pp. 3770–3782, Aug. 2021.

[11] Y.-K. Han, H.-W. Deng, J.-M. Zhu, S.-B. Xing, and W. Han, "Compact dual-band dual-mode SIW balanced BPF with intrinsic common-mode suppression," *IEEE Microw. Wireless Compon. Lett.*, vol. 31, no. 2, pp. 101–104, Feb. 2021.

[12] A. Iqbal, A. W. Ahmad, A. Smida, and N. K. Mallat, "Tunable SIW bandpass filters with improved upper stopband performance," *IEEE Trans. Circuits Syst. II, Exp. Briefs*, vol. 67, no. 7, pp. 1194–1198, Jul. 2020.

[13] A. Iqbal, J. J. Tiang, C. K. Lee, N. K. Mallat, and S. W. Wong, "Dual-band half mode substrate integrated waveguide filter with independently tunable bands," *IEEE Trans. Circuits Syst. II, Exp. Briefs*, vol. 67, no. 2, pp. 285–289, Feb. 2020.

[14] T.-Y. Lin and T.-L. Wu, "Balanced bandpass filter with common-mode reflectionless feature by terminated coupled lines," *IEEE Trans. Electromagn. Compat.*, vol. 62, no. 4, pp. 1090–1097, Aug. 2020.

[15] Y. Zhu, K. Song, M. Fan, S. Guo, Y. Zhou, and Y. Fan, "Wideband balanced bandpass filter with common-mode noise absorption using double-sided parallel-strip line," *IEEE Microw. Wireless Compon. Lett.*, vol. 30, no. 4, pp. 359–362, Apr. 2020.

[16] K. Aliqab and J. Hong, "Wideband differential-mode bandpass filters with stopband and common-mode suppression," *IEEE Microw. Wireless Compon. Lett.*, vol. 30, no. 3, pp. 233–236, Mar. 2020.

[17] R. Gomez-Garcia, L. Yang, and J.-M. Munoz-Ferreras, "Balanced quasi-elliptic-type combline diplexer with multiextracted-pole junction/output sections," *IEEE Microw. Wireless Compon. Lett.*, vol. 30, no. 6, pp. 569–572, Jun. 2020.

[18] A. Fernández-Prieto, A. Lujambio, F. Martín, J. Martel, F. Medina, and R. R. Boix, "Compact balanced-to-balanced diplexer based on split-ring resonators balanced bandpass filters," *IEEE Microw. Wireless Compon. Lett.*, vol. 28, no. 3, pp. 218–220, Mar. 2018.

[19] Y. Zhou, H.-W. Wei, and Y. Zhao, "Compact balanced-to-balanced microstrip diplexer with high isolation and common-mode suppression," *IEEE Microw. Wireless Compon. Lett.*, vol. 24, no. 3, pp. 143–145, Mar. 2014.

[20] A. Fernández-Prieto, A. Lujambio, J. Martel, F. Medina, F. Martín, and R. R. Boix, "Balanced-to-balanced microstrip diplexer based on magnetically coupled resonators," *IEEE Access*, vol. 6, pp. 18536–18547, 2018.

[21] Y. Song, P. Wen, H. Liu, Y. Wang, and L. Geng, "Design of compact balanced-to-balanced diplexer using dual-mode CRLH resonator for RFID and 5G applications," *IEEE J. Radio Freq. Identificat.*, vol. 3, no. 3, pp. 143–148, Sep. 2019.
[22] F. Wei, X. Y. Cheng, Y. X. Liu, and X. W. Shi, "Balanced-to-balanced diplexer and quadruplexer with high selectivity and wide CM suppression," *IEEE Trans. Circuits Syst. II, Exp. Briefs*, vol. 67, no. 11, pp. 2467–2471, Nov. 2020.
[23] X. Liu, Z. Zhu, Y. Liu, Q. Lu, X. Yin, and Y. Yang, "Compact bandpass filter and diplexer with wide-stopband suppression based on balanced substrate-integrated waveguide," *IEEE Trans. Microw. Theory Techn.*, vol. 69, no. 1, pp. 54–64, Jan. 2021.
[24] Y. C. Li, D.-S. Wu, Q. Xue, and B.-J. Hu, "Miniaturized single-ended and balanced dual-band diplexers using dielectric resonators," *IEEE Trans. Microw. Theory Techn.*, vol. 68, no. 10, pp. 4257–4266, Oct. 2020.
[25] K. Song, J. Yao, Y. Chen, Y. Zhou, Y. Zhu, and Y. Fan, "Balanced diplexer based on substrate integrated waveguide dual-mode resonator," *IEEE Trans. Microw. Theory Techn.*, vol. 68, no. 12, pp. 5279–5287, Dec. 2020.
[26] A. Iqbal, J. J. Tiang, C. K. Kee, and B. M. Lee, "Tunable substrate integrated waveguide diplexer with high isolation and wide stopband," *IEEE Microw. Wireless Compon. Lett.*, vol. 29, no. 7, pp. 456–458, Jul. 2019.
[27] X. Guo, L. Zhu, and W. Wu, "Balanced diplexers based on inner-coupled dual-mode structures with intrinsic common-mode suppression," *IEEE Access*, vol. 5, pp. 26774–26782, 2017.
[28] H. Chan, C. Lee, and C. G. Hsu, "Balanced dual-band diplexer design using microstrip and slot-line resonators," in *Proc. Asia–Pacific Microw. Conf. (APMC)*, vol. 3, Dec. 2015, pp. 1–3.
[29] W. Jiang, Y. Huang, T. Wang, Y. Peng, and G. Wang, "Microstrip balanced quad-channel diplexer using dual-open/short-stub loaded resonator," in *IEEE MTT-S Int. Microw. Symp. Dig.*, May 2016, pp. 1–3.
[30] C.-H. Lee, C.-I. G. Hsu, S.-X. Wu, and P.-H. Wen, "Balanced quad-band diplexer with wide common-mode suppression and high differential-mode isolation," *IET Microw., Antennas Propag.*, vol. 10, no. 6, pp. 599–603, Apr. 2016.
[31] R. Gomez-Garcia, J.-M. Munoz-Ferreras, L. Yang, and D. Psychogiou, "Contiguous-channel dual-band balanced diplexer," *IEEE Microw. Wireless Compon. Lett.*, vol. 29, no. 5, pp. 318–320, May 2019.
[32] J. L. M. del Rio, A. Lujambio, A. Fernández-Prieto, A. J. Martinez-Ros, J. Martel, and F. Medina, "Multilayered balanced dual-band bandpass filter based on magnetically coupled open-loop resonators with intrinsic common-mode rejection," *Appl. Sci.*, vol. 10, no. 9, p. 3113, Apr. 2020.
[33] J.-S. Hong, *Microstrip Filters for RF/Microwave Applications*. New York, NY, USA: Wiley, 2011.
[34] A. Fernández-Prieto, A. Lujambio, J. Martel, F. Medina, F. Mesa, and R. R. Boix, "Simple and compact balanced bandpass filters based on magnetically coupled resonators," *IEEE Trans. Microw. Theory Techn.*, vol. 63, no. 6, pp. 1843–1853, Jun. 2015.
[35] Keysight. *Pathwave Advanced Design System (ADS)*. [Online]. Available: https://www.keysight.com/es/en/products/software/pathwave-design-software/pathwave-advanced-design-system.html

JOSE L. MEDRÁN DEL RÍO (Graduate Student Member, IEEE) was born in Puertollano, Ciudad Real, Spain, in 1994. He received the bachelor's degree in telecommunication technologies and services engineering, the master's degree in telecommunication technologies, systems and networks, and the master's degree in telecommunication engineering from the Universitat Politècnica de València, in 2016, 2018, and 2019, respectively. He is currently pursuing the Ph.D. degree with the Electronics and Electromagnetism Department, Universidad de Sevilla, Seville, Spain. His research interest includes new configurations of planar differential microwave devices for multiband applications.

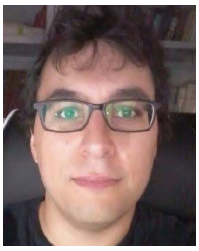

ARMANDO FERNÁNDEZ-PRIETO (Senior Member, IEEE) was born in Ceuta, Spain, in September 1981. He received the Licenciado and Ph.D. degrees in physics from the Universidad de Sevilla, Seville, Spain, in 2007 and 2013, respectively. He is currently an Associate Professor of electromagnetism with the Department of Electronics and Electromagnetism, University of Seville, and a member of the Microwaves Group. His research interests include printed passive microwave components and metamaterials.

JESÚS MARTEL (Senior Member, IEEE) received the Licenciado and Ph.D. degrees in physics from the University of Sevilla, Seville, Spain, in 1989 and 1996, respectively. Since 1990, he has been researching with the Microwave Group, University of Sevilla. He is currently a Professor with the Department of Applied Physics II, University of Sevilla, where he was the Head of the Department, from 2010 to 2018. His current research interests include the numerical analysis of planar transmission lines, the modeling of planar microstrip discontinuities, the design of passive microwave circuits, the techniques in microwave measurements, and the proprieties of artificial media.

RAFAEL R. BOIX (Member, IEEE) received the Licenciado and Ph.D. degrees in physics from the University of Seville, Spain, in 1985 and 1990, respectively. Since 1986, he has been with the Electronics and Electromagnetism Department, University of Seville, where he became a Tenured Professor, in 2010. He belongs to the Microwaves Group, University of Seville. His current research interests include the efficient numerical analysis of periodic planar multilayered structures with applications to the design of frequency selective surface and reflectarray antennas, and on the development of circuit approaches for the synthesis of microstrip antennas with frequency selective response.

FRANCISCO MEDINA (Fellow, IEEE) was born in Puerto Real, Cádiz, Spain, in 1960. He received the Licenciado and Ph.D. degrees in physics from the Universidad de Sevilla, Spain, in 1983 and 1987, respectively. He is currently a Professor in electromagnetism with the Department of Electronics and Electromagnetism, Universidad de Sevilla, where he is also the Head of the Microwaves Group. His current research interests include analytical and numerical methods for planar structures, anisotropic materials, artificial media modeling, and planar microwave circuits. He has published a number of book chapters, journal articles, and conference papers on these topics. He is the Editor-in-Chief of the *International Journal of Microwave and Wireless Technologies*.